Sequence Specific Assignment and Determination of OSR1 *C*-terminal Domain Structure by NMR

Mubarak A. AlAmri,[1,2] Mark Jeeves[*,3] and Youcef Mehellou[*,4]

[1]School of Pharmacy, College of Medical and Dental Sciences, University of Birmingham, Edgbaston, Birmingham B15 2TT, U.K.

[2]Department of Pharmaceutical Chemistry, College of Pharmacy, Prince Sattam Bin Abdulaziz University, Alkharj 11942, Saudi Arabia.

[3]Henry Wellcome Building for NMR, Institute of Cancer and Genomic Sciences, University of Birmingham, Edgbaston, Birmingham B15 2TT, U.K.

[4]Cardiff School of Pharmacy and Pharmaceutical Sciences, King Edward VII Avenue, Cardiff University, Cardiff CF10 3NB, U.K.

Corresponding authors: m.jeeves@bham.ac.uk (MJ); MehellouY1@cardiff.ac.uk (YM).

Abstract

The binding of SPAK and OSR1 kinases to their upstream WNK kinases is mediated by the interaction of their highly conserved SPAK and OSR1 *C*-terminal domain (CTD) to RFx[V/I] peptide sequences from WNK kinases. A SPAK CTD knock-in mouse, where SPAK was unable to bind WNK kinases, exhibited low blood pressure. This highlighted the inhibition of SPAK and OSR1 kinases binding to their upstream WNK kinases as a plausible strategy in the discovery of new antihypertensive agents. To facilitate such endeavour, we herein report the optimisation and expression of isotopically labelled OSR1 CTD in *E.coli* and a structural model based on the sequence specific NMR assignments giving insights into the structure of apo OSR1 CTD. Additionally, we identified the OSR1 CTD amino acid residues that are important for the binding of an 18-mer RFQV peptide derived from human WNK4. Collectively, the NMR backbone assignments and the generated OSR1 CTD 3D model reported in this work will be a powerful resource in the NMR-based discovery of small molecule OSR1 (and SPAK) kinase inhibitors as potential antihypertensive agents.

Keywords: OSR1, SPAK, Kinase, NMR, Assignment.

1. Introduction

STE20/SPS1-related proline/alanine-rich kinase (SPAK) and the oxidative-stress-responsive kinase 1 (OSR1) are two serine/threonine protein kinases that play important roles in regulating ion homeostasis and blood pressure [1, 2]. SPAK and OSR1 share 68% sequence identity and both have an *N*-terminal kinase domain and a 92-amino acids highly conserved *C*-terminal domain (CTD) [3]. SPAK and OSR1 become activated under osmotic stress via phosphorylation at a highly conserved T-loop threonine residue, T185 for human OSR1 and T233 for human SPAK, by known lysine (WNK) kinases [4, 5]. Once phosphorylated, SPAK and OSR1 form heterodimeric complexes with an adaptor protein known as mouse only protein 25 (MO25), of which two isoforms exist in humans (MO25α and β) [6]. Subsequently, SPAK and OSR1 in complex with MO25 phosphorylate an array of sodium, potassium and chloride ion co-transporters, such as NKCC1/2, NCC and KCC, leading to either their activation or inhibition [1, 2].

Various mouse models have indicated that the inhibition of SPAK and OSR1 kinases results in a reduction of blood pressure [7]. Among these was a mouse model with a knock-in mutation in the SPAK CTD, which prevented the binding of SPAK to the upstream WNK kinases through its CTD [8]. This was expected since the CTD of SPAK and OSR1 kinases acts as a docking site for the arginine-phenylalanine-glutamine-valine/isoleucine tetrapeptides (RFQV) of WNK kinases [9]. This binding was confirmed by a co-crystal structure of OSR1 CTD in complex with a GRFQVT peptide derived from WNK4 [9]. Together, this provided compelling evidence that the inhibition of SPAK and OSR1 kinases binding to their upstream WNK kinases leads to a lowering in blood pressure. Additionally, it highlighted the site where the RFQV peptide docks onto the SPAK and OSR1 CTD as an attractive molecular target for the discovery of antihypertensive SPAK and OSR1 CTD binders. To capitalize on this observation, and driven by the fact that no apo structure of SPAK or OSR1 CTD has been reported to date, we used NMR to generate a data driven model of OSR1 CTD in solution. Subsequently, we used the NMR assignments and the structure generated to identify the amino acid residues that are involved in the binding of the 18-mer WNK4-derived RFQV peptide.

2. Materials and methods

2.1 Reagents

pGEX-6P-1-OSR1 (433-end) [DU10096] cDNA was purchased from the MRC Reagents and Services, University of Dundee. Glucose, isopropyl *β-D*-1-thiogalactopyranoside and ampicillin were purchased from Sigma-Aldrich. Ammonium-^{15}N chloride and *D*-Glucose[U-^{13}C] were purchased from CK Isotopes Ltd. The 18-mer WNK4-derived RFQV peptide was purchased from GLS Peptide Synthesis (China).

2.2 Expression and purification of isotopically labelled OSR1 CTD

The pGEX-6P-1 construct encoding *N*-terminal GST-tagged OSR1 (433-end) was transformed into BL21 (DE3) *E. coli* cells. Cells were grown in M9 minimal media, in which ammonium-^{15}N chloride and *D*-Glucose-[U-^{13}C] were used as sole sources of nitrogen and carbon, supplemented with 100 µg/mL ampicillin and grown in an incubator shaker at 37 °C at 180 rpm and left to grow until the optical density at 600 nm (OD_{600}) reached 0.6-0.7. Protein expression was then induced by the addition of 250 µM isopropyl-*D*-galactosidase (IPTG). Cells were cultured for additional 16 hours in an incubator shaker at 18 °C at 180 rpm. Proteins were then purified and the GST removed using cleavage by PreScission protease enzyme as described previously [6].

2.3 Backbone assignment of the sequence-specific ^{1}H, ^{13}C and ^{15}N backbone resonance of the human OSR1 CTD

Triple resonance NMR experiments for backbone assignment of OSR1 CTD were performed on a Bruker Avance III 600 MHz spectrometer equipped with 1.7 mm z-axis gradient TCI CryoProbe at 298 K. Backbone assignments were achieved by a combination of 3D backbone assignment experiments, specifically HNCA, HNCO, HNCACO, HN(CO)CA, HNCACB, HN(CO)CACB experiments [10, 11], as well as the 2D ^{1}H, ^{15}N-HSQC [12] . Experiments were run on 0.2 mM uniformly ^{13}C- and ^{15}N-labelled OSR1 CTD in buffer containing 50 mM Tris-d_{11} pH 7.4, 150 mM NaCl and 1 mM dithiothreitol (DTT). Sequence-specific assignment data was processed by NMRPipe [13] and analysed using CcpNmr Analysis [14].

2.4 Mapping the RFQV binding residues by Chemical Shift Perturbations (CSPs)

To assess the RFQV peptide binding to OSR1 CTD and define residues key to the interaction, ^{1}H,^{15}N-HSQC spectra were acquired on 0.2 mM ^{15}N-OSR1 CTD in the absence (apo-protein) and presence of 50 µM RFQV peptide. Subsequently the two spectra were overlaid to observe specific residue CSPs and map these residues to OSR1 CTD backbone assignment. Data were processed by NMRPipe [13] and analysed using CcpNmr Analysis [14]. A filtered NOESY experiment [15] was performed to identify interactions between the peptide and the protein using a sample containing 0.1 mM ^{13}C,^{15}N-labelled OSR1 CTD and 50 µM 18-mer RFQV peptide. NOEs between the protein and the peptide were used together with the CSPs to create a model of the 18-mer RFQV-peptide OSR1 CTD complex using the HADDOCK2.2 webserver [16]. For this model, the crystal structure was stripped of its peptide and then the longer peptide was docked using the NMR restraints. The peptide was allowed to be completely flexible as were those regions of the protein not in secondary structure and all protein side-chains.

2.5 Analysis of CSPs

CSPs (Δδ) in the backbone amide were calculated for each residue in the ^{1}H,^{15}N-NMR HSQC spectra according to the following equation:

$$\Delta\delta\,(\mathrm{H},\mathrm{N}) = \sqrt{(\Delta\delta\mathrm{H})^2 + (0.154\ x\ \Delta\delta\mathrm{N})^2}$$

Where ΔδH and ΔδN are the ^{1}H and ^{15}N amide chemical shift changes, in ppm, induced by the binding of ligand and resulting conformational changes. CSPs (Δδ) were defined as the difference between the corresponding chemical shifts in the bound (δ_{bound}) and free (δ_{free}) states of the OSR1 CTD [17].

2.6 OSR1 CTD secondary structure prediction based on NMR chemical shifts

The secondary structure of OSR1 CTD was predicted by TALOS+ (torsion angle likelihood obtained from shift and sequence similarity) server (https://spin.niddk.nih.gov/bax/software/TALOS)[18] and CSI (chemical shift index) server (http://csi3.wishartlab.com)[19] using NMR chemical shifts of Hn, Cα, Cβ and C' nuclei.

2.7 Predication of OSR1 CTD 3D structure

The 3D structure of OSR1 CTD was modelled using Chemical-Shift-ROSETTA (CS-Rosetta) server (https://csrosetta.bmrb.wisc.edu/csrosetta/submit) based on OSR1 CTD NMR chemical shifts [20]. OSR1 CTD NMR chemical shifts were obtained from the output from TALOS+ server. The model with best RMDS score was used for further discussion.

3. Results and Discussion

3.1. Suitability of OSR1 CTD for NMR studies

In order to assess the suitability of OSR1 CTD for NMR studies, we initially obtained the ^{1}H,^{15}N-HSQC NMR spectrum of the apo ^{15}N-OSR1 CTD (**Supporting Figure S1**) [21]. The results showed that the ^{15}N-isotopically labeled OSR1 CTD was expressed in a folded form as illustrated by the wide dispersion of the amide resonance peaks (6.5–10 ppm) in the ^{1}H-dimension. The uniform intensity of most of the amide resonance peaks suggested that the domain existed in a single stable conformation. The number of the resolved backbone amide resonance peaks observed in the ^{1}H,^{15}N-HSQC spectrum of OSR1 CTD of OSR1 was 92 cross peaks, which represents 100% of the total number of amino acid residues in this protein fragment. In addition, few weak peaks were observed just above the noise level, which were assumed to be from flexible residues on the linker left over after cleavage of the GST tag. Overall, the results indicated that the OSR1 CTD was suitable for NMR studies.

3.2. Assignment of OSR1 CTD

Sequence specific backbone assignment of OSR1 CTD was carried out in order to assign each spin system with its corresponding residue within the OSR1 CTD amino acid sequence. ^{13}C and ^{15}N-labelled OSR1 CTD was expressed and purified from *E. coli* (**Supporting Figure S2**). The backbone amide resonances of 77 residues were assigned, representing 88% of the total 88 non-proline amino acid residues (**Figure 1A**). Of the assigned amino acids, 100% include Cα, 91% include Cβ and 99% C' chemical shifts. Due to intermediate exchange and broadening of the resonances, the assignment of the amide resonances of residues Ile434, Val437, Ser433, Gly457, Ala461, Ser498, Val499, Ser510,

Asp511, Ile512 and Ser525 was not possible. Mapping the location of these unassigned residues onto the reported crystal structure of OSR1 CTD (PDB: 2V3S) revealed that some of these residues (510-513) are located in flexible loop regions (**Figure 1B**) which likely results in reduced peak intensity, whilst others could not be assigned unambiguously due to the overlap of the carbon chemical shifts. Chemical shift assignments have been deposited in the BMRB database (Accession number: 27834).

A.

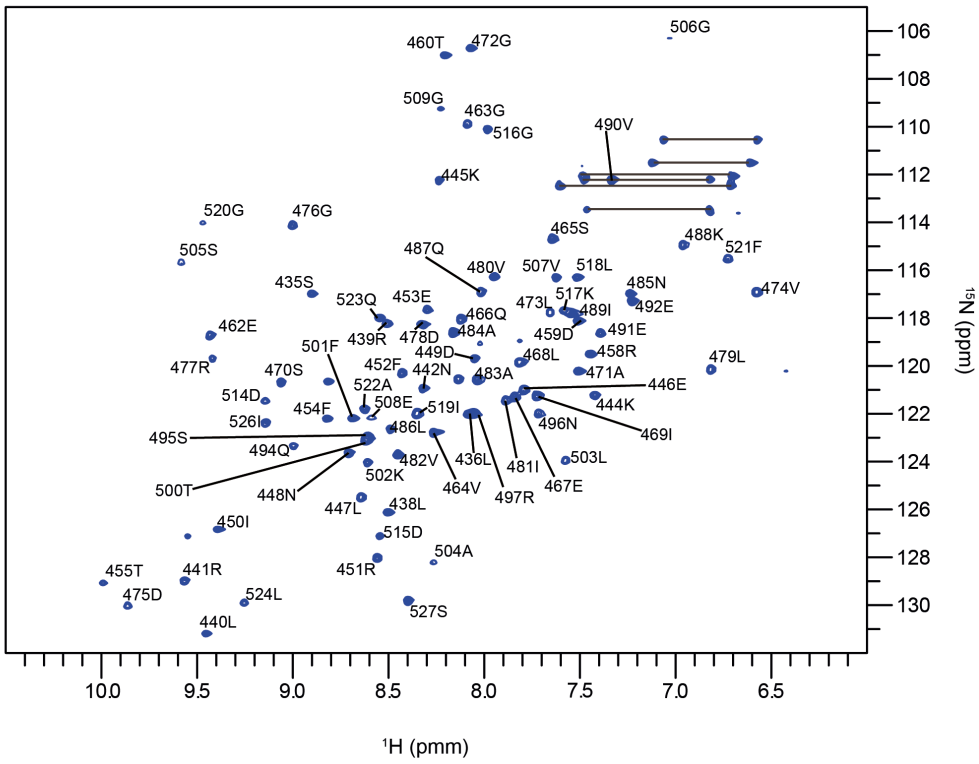

B.

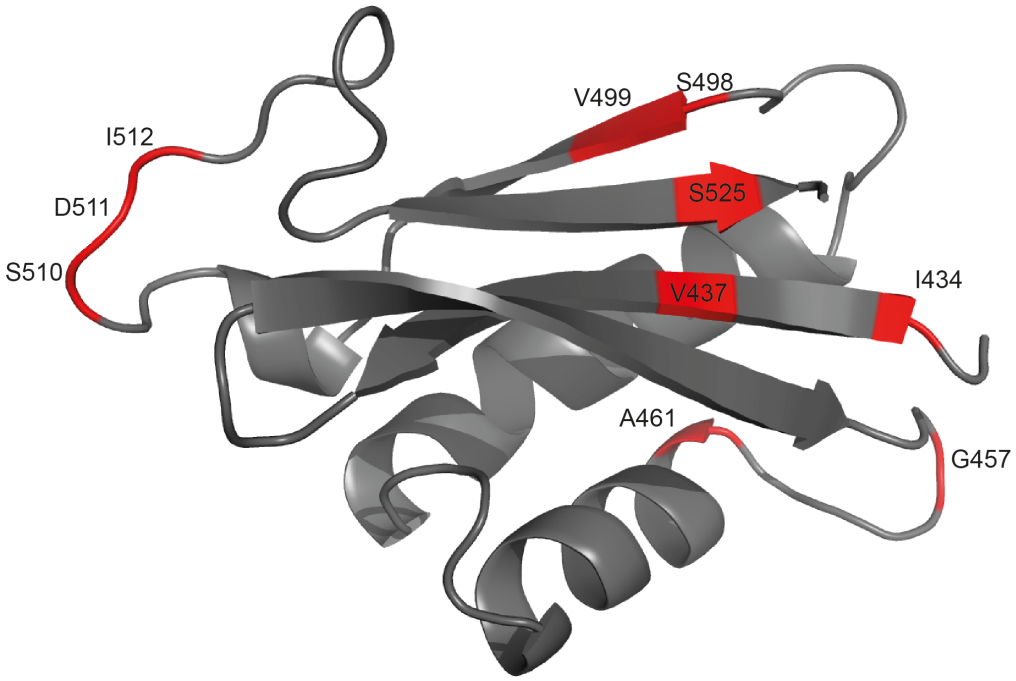

Figure 1. Assignment of the OSR1 CTD NMR structure. (**A**) ^{11}H, ^{5}N-HSQC of ^{13}C,^{15}N-labelled OSR1 CTD. OSR1 CTD peaks are labelled with their assignments. Side chains amides from glutamine and asparagine residues are indicated by horizontal lines between the two proton resonances. Unassigned residues are not labelled. (**B**) Mapping unassigned residues onto OSR1 CTD crystal structure (PDB: 2V3S). Regions in red correspond to unassigned amide resonances.

3.3. Determination of OSR1 CTD secondary structure

The secondary structure of OSR1 CTD was determined using TALOS+ (torsion angle likelihood obtained from shift and sequence similarity)[18] and CSI (chemical shift index) webservers[19]. Both servers required the NMR assignments of certain nuclei for empirical prediction of the dihedral angles phi and psi. A comparison of OSR1 CTD secondary structure predicted by TALOS+ with the secondary structure defied by the OSR1 CTD crystal structure revealed that both structures have the same number and type of secondary structure elements with few differences in the *C*-terminal region (**Figure 2A**). A major difference was that the NMR chemical shift analysis does not predict α3. In the case of CSI (chemical shift index), the alpha helix (α3) is replaced by a turn (**Figure 2B**) whereas TALOS+ does not predict any secondary structure. The backbone N, H_N, Cα, C' and Cβ of the amino acid residues corresponding to the α3 helix in the crystal structure (Ala505, Ser506, Gly507, Val508, Glu509) are assigned. Our results provided a new insight into the structure of OSR1 CTD in solution and suggest that in the apo form of OSR1 any secondary structure in the loop between β3 and β4 is likely to be transient and that the loop is likely to have significant flexibility.

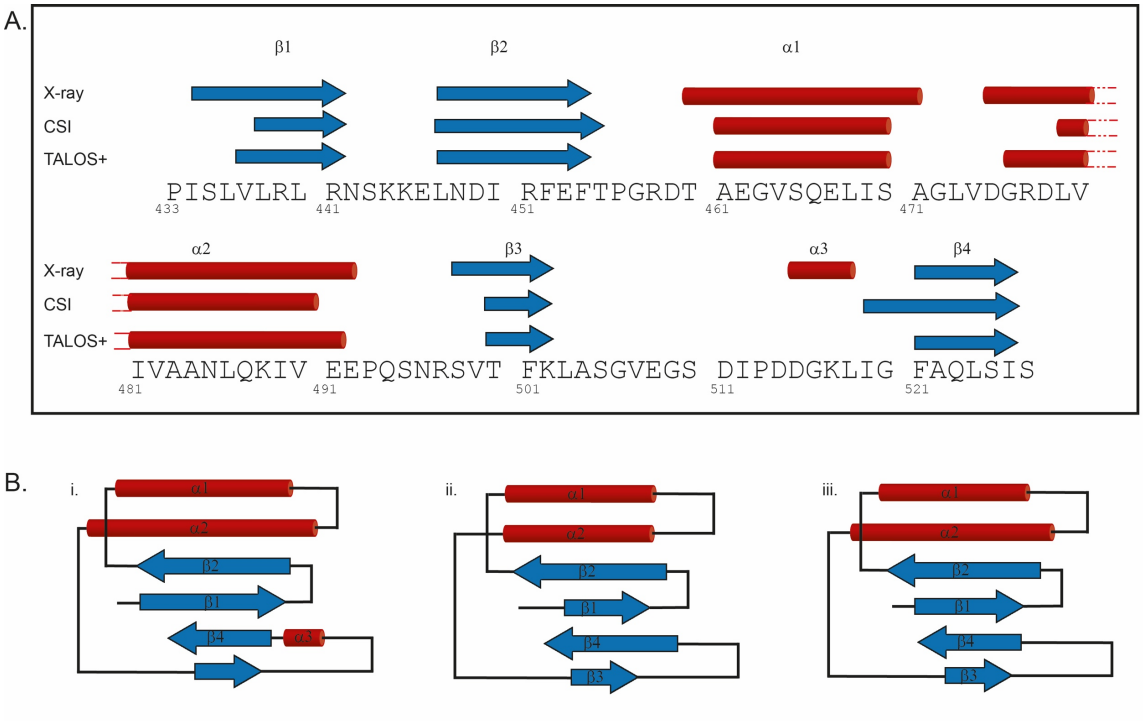

Figure 2. OSR1 CTD secondary structure. (**A**) The secondary structure of OSR1 CTD based on the X-

ray structure (PDB: 2V3S) and NMR chemical shift information interpreted by CSI and TALOS+ webservers). (**B**) The strand pairing of the peptide bound X-ray crystal structure (i) and the likely strand pairing of the apo structure based on CSI (ii) and Talos(iii).

3.4. Determination of OSR1 CTD tertiary structure by CS-Rosetta.

The Chemical-Shift-Rosetta (CS-Rosetta) webserver was used to build a model of the CTD of OSR1 structure using the NMR chemical shift data [20]. The best model structure of CTD of OSR1 with lowest energy score among the ten best models obtained by CS-Rosetta is shown in (**Figure 3**)**.** A comparison of our CS-Rosetta 3D models of CTD of OSR1 with the OSR1 crystal structure [9] indicated that both structures were very similar in their folding pattern with some differences that are notable particularly in the *C*-terminal region. The loop region between strands β3 and β4 is highly variable in the different Rosetta models and the helix seen in the crystal structure is rarely seen (**Figure 2A**). This region forms a long loop that is involved in the formation of the secondary pocket. However, the backbone assignments of the main residues that form α4 (Ser510, Asp511 and Ile512) residues are incomplete suggesting that region is in dynamic exchange and any secondary structure formed is likely to be transient. This flexibility may be more pronounced in the apo form of CTD of OSR1 studied here rather than the peptide bound structure seen in the crystal. The lack of complete NMR assignment in this region may also be responsible for the observed variation in the orientation and structure of β4 of the OSR1 CTD, which is highly variable in the different Rosetta models. This *C*-terminal region is sometimes seen to form an alpha helix, an external β-strand (meaning that β2 and β3 are parallel with β4 outside and antiparallel to β3) or and internal antiparallel β-strand between β2 and β3 (as observed in the crystal structure). Therefore, this should be noted when considering the predicted arrangement of this region. As the CSI interpretation of the chemical shift data predicts that this region forms an internal β-strand, it is likely that the strand orientation seen in the crystal structure is the one seen in the apo solution state. The location of a short alpha helix between α2 and β3 in the many of the predicted models is consistent with the weak prediction of a helix by TALOS+. It is likely that this helix is transiently formed to maintain some order to this extended loop region.

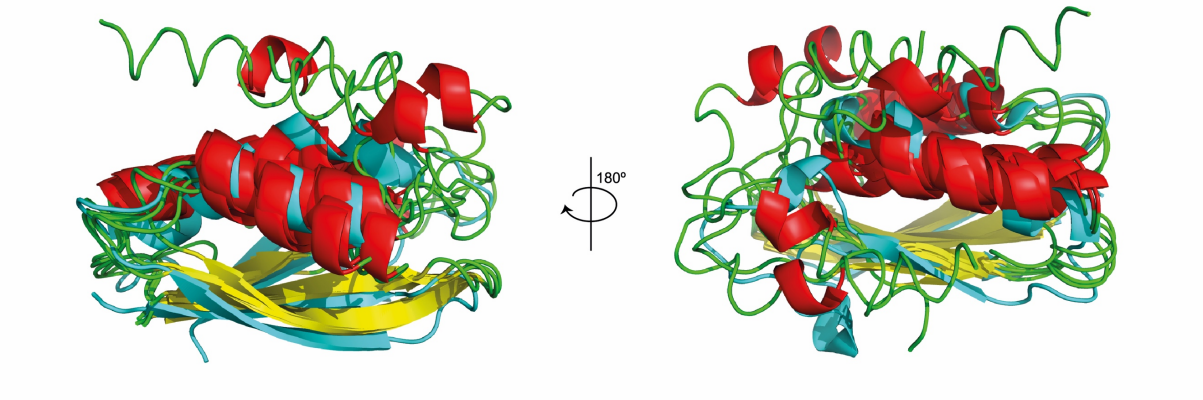

Figure 3. Predicted structures of OSR1 CTD based on NMR assignment. A ribbon representation of the five lowest energy models generated by CS-Rosetta webserver using data derived from assigned chemical shifts together with the protein from the peptide bound X-ray crystal structure (PDB: 2V3S). The figure was prepared using PyMOL Molecular Graphics System 1.3.

The structures are aligned using the Cα atoms in the first two β-strands which are well converged in the models. The *C*-terminal region (A503-S527) is highly variable in the Rosetta models indicative of the flexible nature of parts this region. Some secondary structure is present in this region, especially in residues 515-526, but the β-strand seen in this region in the X-ray structure is not always present in the Rosetta models often replaced by an α-helix. The complex turns seen in the X-ray structure of the peptide complex are not replicated partly due to the lack of assignments of residues 510-512. These missing assignments are likely due line broadening caused by conformational exchange in this loop region suggesting that this region is dynamic in the apo protein in solution.

3.5. Mapping the binding of the RFQV peptide to OSR1 CTD

In order to identify those residues of OSR1 CTD responsible for WNK4 interaction, we next incubated 0.2 mM OSR1 CTD with 50 μM of the 18-mer RFQV peptide that is derived from human WNK4 (aa. 1006-1020). The sample was then studied by acquiring a ^{1}H, ^{15}N-HSQC spectrum. The results showed that the 18-mer RFQV peptide induced large CSPs when it was added to OSR1 CTD even at sub-stoichiometric quantities (**Figure 4A**). Interestingly, some peaks, e.g., Arg451, could no longer be observed when the RFQV peptide was added indicting that this residue is either involved in dynamic exchange events or that it shifts so far that it cannot be identified unambiguously. Pronounced line broadening is observed in some residues, e.g., F454 and L468, in addition to the chemical shift perturbation, indicating that there is exchange between the bound and unbound forms at an intermediate rate on the NMR timescale. The CSPs were quantified and divided into three levels; small, medium and large based on the amplitude of the CSP. Accordingly, twelve residues were perturbed by

a large amount upon addition of the 18 mer RFQV peptide. These were L440, N448, I450, F452, E453, F454, Q467, L468, A471, L473, A483 and F501 (**Supporting Figure S3**). Most of these residues are located in the vicinity of the interaction site seen in the crystal structure of the complex OSR1 CTD and validated in mutagenesis studies [9]. Residues L440 and N448 are outside of the primary binding site seen in the crystal structure suggesting that the longer peptide used in this study forms a longer β-augmentation with strand β2. This is supported by the model generated using HADDOCK which shows that the interaction between the peptide and protein exceeds the RFQV motif (**Figure 4B**). In the HADDOCK generated model, it can clearly be seen how F452 and F454 form a pocket for the phenylalanine in the RFQV motif. R451 lies on the edge of the binding site and this leads to only a weak interaction of this residue with the peptide resulting in the disappearance of the peak in the HSQC. The large perturbations seen in residues F501 and A483, which lie away from the binding surface, indicate how the effects of peptide binding could be transmitted through the rest of the protein structure.

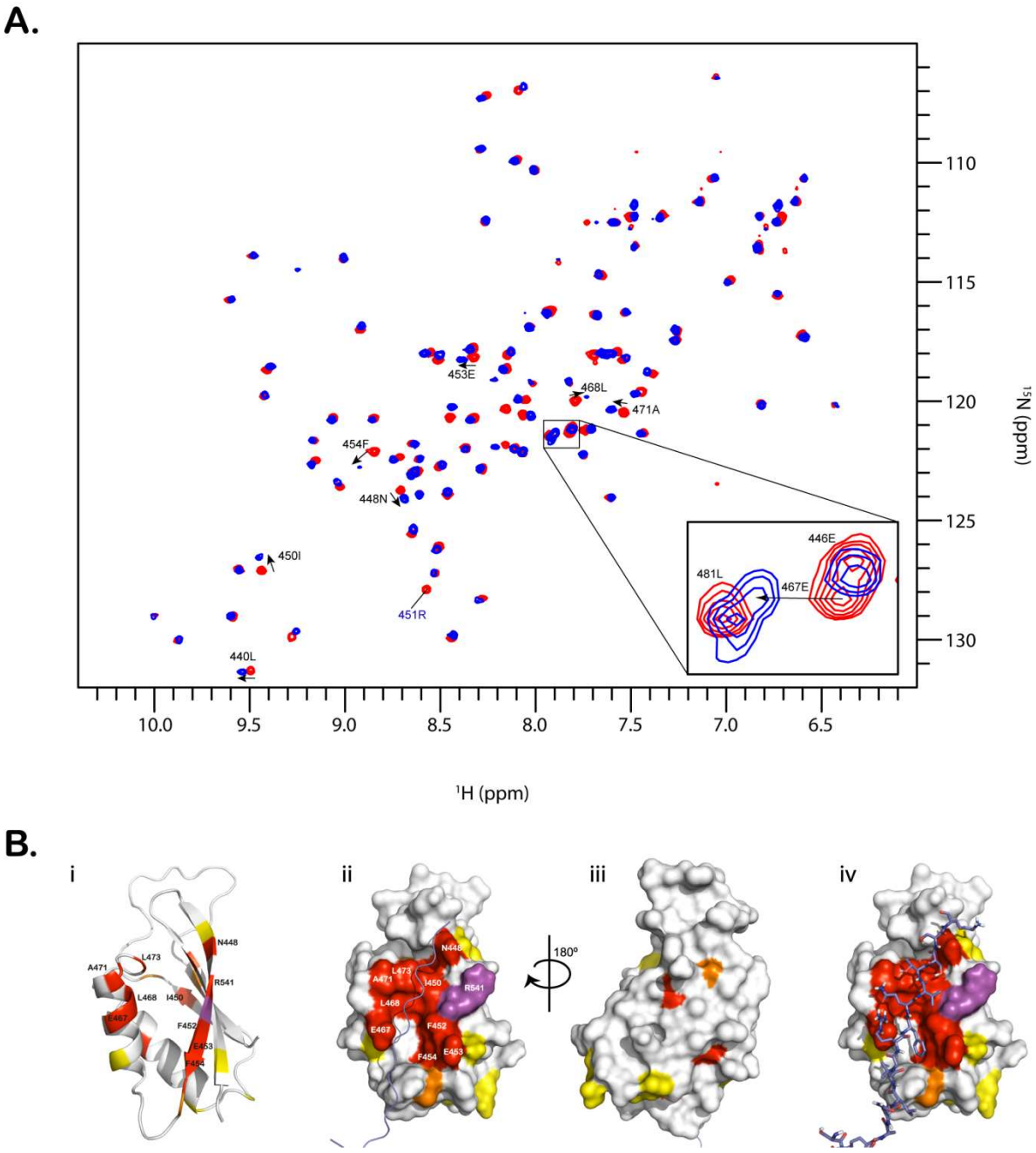

Figure 4. RFQV binding to OSR1 CTD. (**A**) CSPs following the addition of RFQV peptide to ^{15}N-labelled OSR1 CTD. The ^{1}H, ^{15}N- HSQC spectrum of free OSR1 CTD (apo-protein) and after the addition of 50 µM RFQV peptide are shown in blue and red, respectively. Selected residues with large CSPs are labelled. The region around Glu467 residue is further expanded. Arg451 (labelled in blue) can no longer be observed when the RFQV peptide was added. (**B**) CSPs mapped on to the model of OSR1 CTD bound to the 18mer RFQV peptide created by HADDOCK in a ribbon representation (i), OSR1 CTD, a surface representation in the same orientation with the peptide shown in ribbon form (ii), a surface representation rotated by 180° around a vertical axis (iii) and with the bound RFQV peptide shown in stick form (iv). Chemical shift perturbations are color coded with residues in red showing the largest

perturbations, orange medium perturbations and yellow small perturbations. Arg451, whose amide resonances could not be identified in the HSQC of the complex, is indicated in purple.

In summary, we herein reported the first OSR1 CTD apo structure using NMR. The sequence specific assignments of the isotopically labelled OSR1 CTD were used to identify the amino acid residues that are important in the binding of OSR1 to an 18-mer RFQV peptide, which is derived from the protein kinase WNK4, an OSR1 protein binder. The binding of the peptide to OSR1 CTD caused shifts in eighteen amino acid residues including some that were previously noted as being important for binding this peptide. Given that OSR1 CTD, and that of its closely related kinase SPAK, are the molecular targets for the discovery of small molecule antihypertensive agents, our reported NMR assignments and structural model represents a powerful resource that will facilitate the NMR-based discovery of small molecule SPAK and OSR1 CTD binders.

Conflict of interests

The authors declare that they have no conflicting interests.

References

1 Alessi, D. R., Zhang, J., Khanna, A., Hochdorfer, T., Shang, Y. and Kahle, K. T. (2014) The WNK-SPAK/OSR1 pathway: master regulator of cation-chloride cotransporters. Sci Signal. **7**, re3

2 Hadchouel, J., Ellison, D. H. and Gamba, G. (2016) Regulation of Renal Electrolyte Transport by WNK and SPAK-OSR1 Kinases. Annu Rev Physiol. **78**, 367-389

3 Vitari, A. C., Thastrup, J., Rafiqi, F. H., Deak, M., Morrice, N. A., Karlsson, H. K. and Alessi, D. R. (2006) Functional interactions of the SPAK/OSR1 kinases with their upstream activator WNK1 and downstream substrate NKCC1. Biochem J. **397**, 223-231

4 Vitari, A. C., Deak, M., Morrice, N. A. and Alessi, D. R. (2005) The WNK1 and WNK4 protein kinases that are mutated in Gordon's hypertension syndrome phosphorylate and activate SPAK and OSR1 protein kinases. Biochem J. **391**, 17-24

5 Richardson, C. and Alessi, D. R. (2008) The regulation of salt transport and blood pressure by the WNK-SPAK/OSR1 signalling pathway. Journal of cell science. **121**, 3293-3304

6 Filippi, B. M., de los Heros, P., Mehellou, Y., Navratilova, I., Gourlay, R., Deak, M., Plater, L., Toth, R., Zeqiraj, E. and Alessi, D. R. (2011) MO25 is a master regulator of SPAK/OSR1 and MST3/MST4/YSK1 protein kinases. The EMBO journal. **30**, 1730-1741

7 Murthy, M., Kurz, T. and O'Shaughnessy, K. M. (2017) WNK signalling pathways in blood pressure regulation. Cell Mol Life Sci. **74**, 1261-1280

8 Zhang, J., Siew, K., Macartney, T., O'Shaughnessy, K. M. and Alessi, D. R. (2015) Critical role of the SPAK protein kinase CCT domain in controlling blood pressure. Hum Mol Genet. **24**, 4545-4558

9 Villa, F., Goebel, J., Rafiqi, F. H., Deak, M., Thastrup, J., Alessi, D. R. and van Aalten, D. M. (2007) Structural insights into the recognition of substrates and activators by the OSR1 kinase. EMBO Rep. **8**, 839-845
10 Kay, L. E., Xu, G. Y. and Yamazaki, T. (1994) Enhanced-Sensitivity Triple-Resonance Spectroscopy with Minimal H2o Saturation. J Magn Reson Ser A. **109**, 129-133
11 Muhandiram, D. R. and Kay, L. E. (1994) Gradient-Enhanced Triple-Resonance 3-Dimensional Nmr Experiments with Improved Sensitivity. J Magn Reson Ser B. **103**, 203-216
12 Schleucher, J., Schwendinger, M., Sattler, M., Schmidt, P., Schedletzky, O., Glaser, S. J., Sorensen, O. W. and Griesinger, C. (1994) A General Enhancement Scheme in Heteronuclear Multidimensional Nmr Employing Pulsed-Field Gradients. Journal of biomolecular NMR. **4**, 301-306
13 Delaglio, F., Grzesiek, S., Vuister, G. W., Zhu, G., Pfeifer, J. and Bax, A. (1995) NMRPipe: a multidimensional spectral processing system based on UNIX pipes. Journal of biomolecular NMR. **6**, 277-293
14 Vranken, W. F., Boucher, W., Stevens, T. J., Fogh, R. H., Pajon, A., Llinas, M., Ulrich, E. L., Markley, J. L., Ionides, J. and Laue, E. D. (2005) The CCPN data model for NMR spectroscopy: development of a software pipeline. Proteins. **59**, 687-696
15 Zwahlen, C., Legault, P., Vincent, S. J. F., Greenblatt, J., Konrat, R. and Kay, L. E. (1997) Methods for measurement of intermolecular NOEs by multinuclear NMR spectroscopy: Application to a bacteriophage lambda N-peptide/boxB RNA complex. J Am Chem Soc. **119**, 6711-6721
16 van Zundert, G. C. P., Rodrigues, J. P. G. L. M., Trellet, M., Schmitz, C., Kastritis, P. L., Karaca, E., Melquiond, A. S. J., van Dijk, M., de Vries, S. J. and Bonvin, A. M. J. J. (2016) The HADDOCK2.2 Web Server: User-Friendly Integrative Modeling of Biomolecular Complexes. J Mol Biol. **428**, 720-725
17 Williamson, M. P. (2013) Using chemical shift perturbation to characterise ligand binding. Progress in nuclear magnetic resonance spectroscopy. **73**, 1-16
18 Shen, Y., Delaglio, F., Cornilescu, G. and Bax, A. (2009) TALOS+: a hybrid method for predicting protein backbone torsion angles from NMR chemical shifts. Journal of biomolecular NMR. **44**, 213-223
19 Hafsa, N. E., Arndt, D. and Wishart, D. S. (2015) CSI 3.0: a web server for identifying secondary and super-secondary structure in proteins using NMR chemical shifts. Nucleic acids research. **43**, W370-377
20 Shen, Y., Lange, O., Delaglio, F., Rossi, P., Aramini, J. M., Liu, G., Eletsky, A., Wu, Y., Singarapu, K. K., Lemak, A., Ignatchenko, A., Arrowsmith, C. H., Szyperski, T., Montelione, G. T., Baker, D. and Bax, A. (2008) Consistent blind protein structure generation from NMR chemical shift data. Proceedings of the National Academy of Sciences of the United States of America. **105**, 4685-4690
21 Yee, A., Chang, X., Pineda-Lucena, A., Wu, B., Semesi, A., Le, B., Ramelot, T., Lee, G. M., Bhattacharyya, S., Gutierrez, P., Denisov, A., Lee, C. H., Cort, J. R., Kozlov, G., Liao, J., Finak, G., Chen, L., Wishart, D., Lee, W., McIntosh, L. P., Gehring, K., Kennedy, M. A., Edwards, A. M. and Arrowsmith, C. H. (2002) An NMR approach to structural proteomics. Proceedings of the National Academy of Sciences of the United States of America. **99**, 1825-1830.

Sequence Specific Assignment and Determination of OSR1 *C*-terminal Domain Structure by NMR

Mubarak A. AlAmri,[1,2] Mark Jeeves[*,3] and Youcef Mehellou[*,4]

[1]School of Pharmacy, College of Medical and Dental Sciences, University of Birmingham, Edgbaston, Birmingham B15 2TT, U.K.

[2]Department of Pharmaceutical Chemistry, College of Pharmacy, Salman Bin Abdulaziz University, Alkharj 11942, Saudi Arabia

[3]Henry Wellcome Building for NMR, Institute of Cancer and Genomic Sciences, University of Birmingham, Edgbaston, Birmingham B15 2TT, U.K.

[4]Cardiff School of Pharmacy and Pharmaceutical Sciences, King Edward VII Avenue, Cardiff University, Cardiff CF10 3NB, U.K.

Corresponding authors: m.jeeves@bham.ac.uk (MJ); MehellouY1@cardiff.ac.uk (YM).

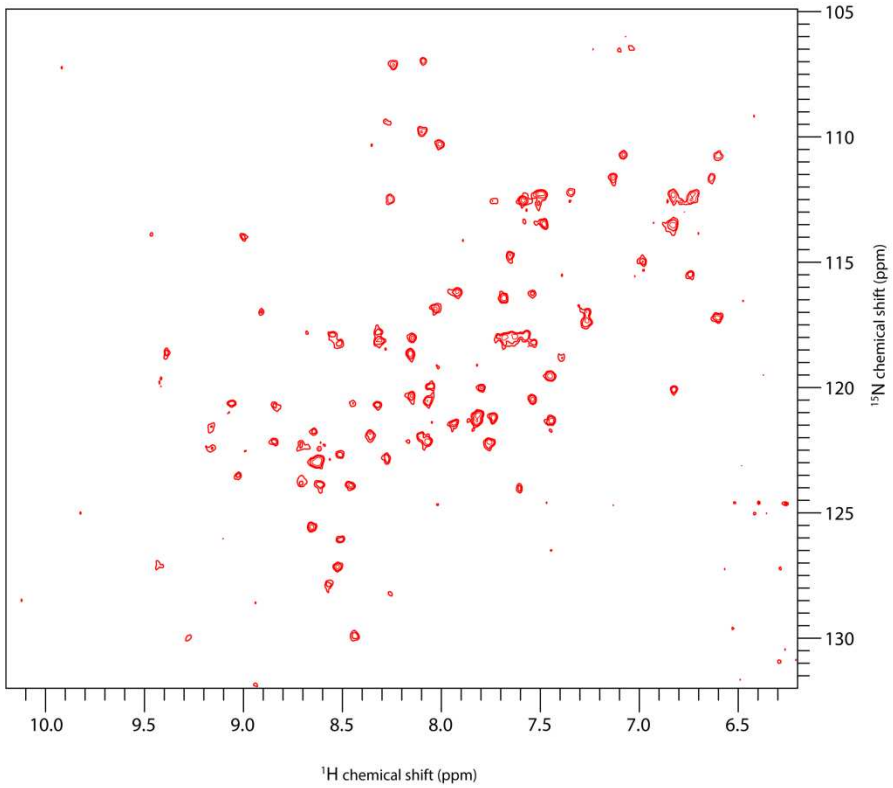

Figure S1: ^{15}N-^{1}H HSQC spectrum of 15N-OSR1 CCT domain. 15N-1H HSQC spectrum of 15N labelled OSR1 CCT domain (0.2 mM) displays strong and even dispersion of amide backbone peaks. 15N-1H HSQC spectrum was recorded in 50 mM Tris-d11 pH 7.4, 150 mM NaCl, 0.1% 2-mercaptoethanol at 25°C on a Bruker 600 MHz NMR spectrometer.

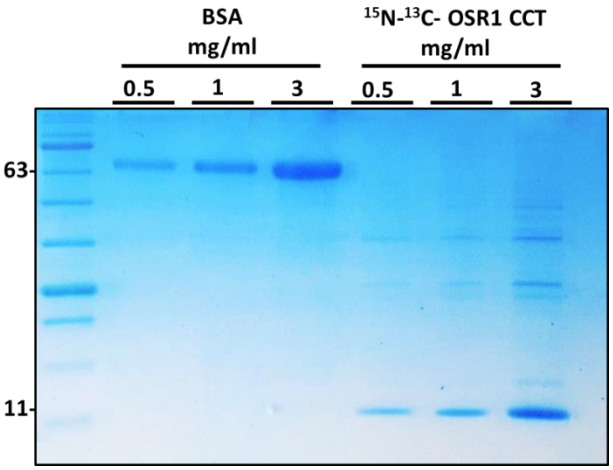

Figure S2: Expression and purification of 15N-13C-OSR1 CCT domain from E.coli. (BSA) Bovine serum albumin (Sigma Aldrich, cat# A2153, purity ≥ 96%) determined by agarose gel electrophoresis) was used at different concentrations as standards for determinations of proteins yield and purity.

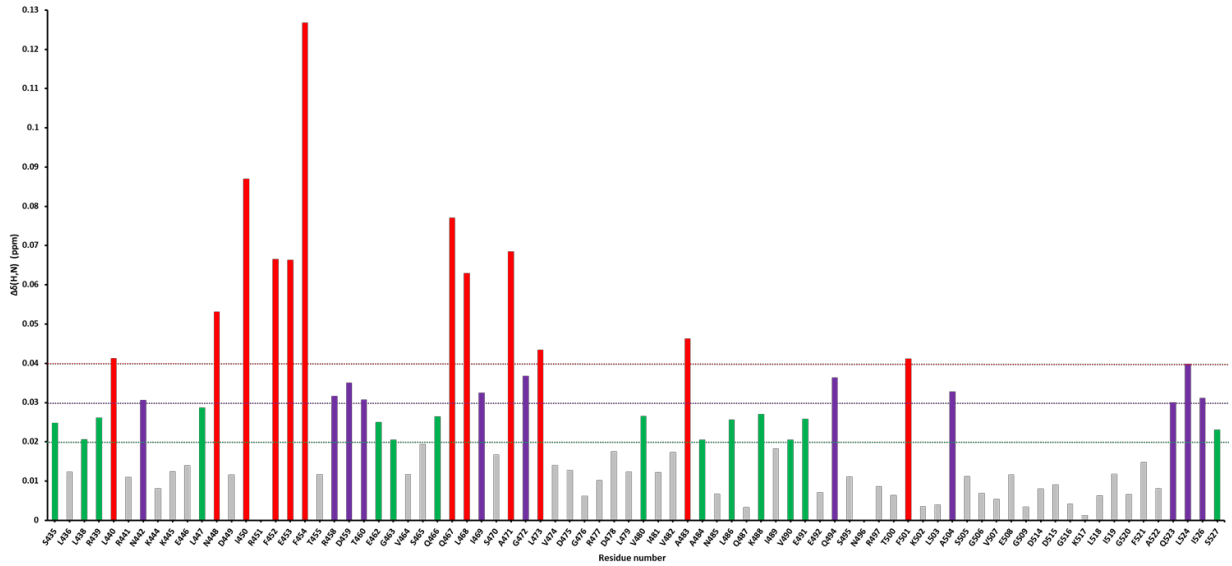

Figure S3: Chemical shift perturbations (CSPs) of human OSR1 CCT domain in presence of 50 µM RFQV peptide. The CSPs are plotted versus residue numbers. The dashed line in red, purple and green show cut-off Δδ > 0.04-, 0.03- and 0.02 ppm indicating large, medium and small chemical shift perturbations, respectively.